Binary Cation Matrix Electrolyte and its Effect on SEI Suppression and Evolution of Si Anode

Journal:	*ACS Applied Materials & Interfaces*
Manuscript ID	am-2024-05194r
Manuscript Type:	Article
Date Submitted by the Author:	29-Mar-2024
Complete List of Authors:	Sa, Niya; University of Massachusetts Boston College of Science and Mathematics, Chemistry Cora, Saida; University of Massachusetts Boston, Chemistry Yang, Zicheng; University of Massachusetts Boston Vaughey, John; Argonne National Lab, Chemical Sciences and Engineering

Binary Cation Matrix Electrolyte and its Effect on SEI Suppression and Evolution of Si Anode

Saida Cora[1], Zicheng Yang[1], John T. Vaughey,[2] Niya Sa[1,*]

[1]*Department of Chemistry, University of Massachusetts Boston, Boston, MA, 02125, United States*

[2]*Chemical Sciences and Engineering Division, Argonne National Laboratory, Lemont, IL, 60439*

ABSTRACT

An unstable solid electrolyte interphase (SEI) has been recognized as one of the biggest challenges to commercializing silicon (Si) anode for high energy density batteries. This work thoroughly investigates a binary cation matrix of Mg^{2+}+Li^{+} electrolyte and its role towards SEI development, suppression, and evolution of a Si anode. Findings demonstrate that introducing Mg ions dramatically reduces the SEI growth before lithiation occurs, primarily due to the suppression of solvent reduction, particularly ethylene carbonate (EC) reduction. The Mg^{2+} alters the Li^{+} cation solvation environment as EC preferably participates in the oxophyllic Mg^{2+} solvation sheath, thereby altering the solvent reduction process, resulting in a distinct SEI formation mechanism. The initial SEI formation before lithiation is reduced by 70% in electrolyte with the presence of Mg^{2+} cations. While the SEI continues to develop in the post-lithiation, the inclusion of Mg ions results in an approximately 80% reduction in the post-lithiation SEI growth. Continuous electrochemical cycling reveals that Mg^{2+} plays a crucial role in stabilizing the deep-lithiated Si phases, which effectively mitigates side reactions, resulting in a controlled SEI growth and stable interphase while eliminating complex Li_xSi_y formation. Mg ions promote the development of a notably more rigid and homogeneous SEI, characterized by a reduced dissipation (ΔD) in the Mg^{2+}+Li^{+} ion matrix compared to the solely Li^{+} system. This report reveals how the Mg^{2+}+Li^{+} ion matrix affects the SEI evolution, viscoelastic properties, and electrochemical behavior at the Si interface in real-time, laying the groundwork for devising strategies to enhance the performance and longevity of Si-based next-generation battery systems.

KEYWORDS: *silicon anode, solid electrolyte interphase, binary cation electrolyte*

1. INTRODUCTION

The ever-increasing demand for energy storage driven by the rapid growth of the electric vehicle market has outpaced the capabilities of the supply chains for current secondary battery technology, particularly the state-of-the-art lithium-ion systems.[1-4] As a result, an ambitious journey is being undertaken to explore alternative environmentally friendly and cost-effective energy storage solutions that provide increased capacity and extended lifespans.[5-7] One promising avenue involves the substitution of conventional graphite anodes with high-capacity main group materials, paving the way for increased energy density.[8-10] Silicon (Si), being both abundant and widely accessible, presents an enticing prospect for cost-effective anode material with exceptional specific capacity (~3640 mAh g^{-1}), far surpassing the capacity of graphite (~370 mAh g^{-1}).[11-14]

The practical utilization of Si as an anode faces notable challenges primarily attributed to the formation of an unstable solid electrolyte interphase (SEI) on the Si anode surface.[15, 16] Understanding the variables that control the SEI stability of Si is paramount as it critically impacts the cyclability, irreversible capacity loss, and safety aspects of lithium-ion batteries (LIBs).[17, 18] The instability of the SEI is a direct consequence of the increased reactivity of the lithiated Si surface towards the electrolyte components, and in tandem with volumetric changes, it results in rapid decay in capacity and a shortened cycle life.[19, 20] Extensive research efforts have been directed towards strategies addressing the challenges of SEI chemistry on Si, for example, designing sacrificial surface layers that protect Si, modifications of electrolyte formulation/additives, nanostructuring, and advanced electrode engineering of Si.[15, 21-26]

One effective and simple strategy to enhance the stability and reduce the reactivity of lithiated Si involves the *in situ* electrochemical formation of Li-M-Si (M = Mg, Al, Ca, Zn) ternary Zintl phases.[27-30] The simplicity of this approach presents introduction of a multivalent cation salt as a secondary component in the conventional Li electrolyte, promising advancements in structural integrity and performance enhancement for Si anodes.[31, 32] Previous post-electrochemical *ex situ* analysis investigated SEI at the Li-M-Si Zintl-phase interface suggesting that improved interphase stability and ion diffusion can be achieved through the formation of the inorganic-rich SEI with multivalent cation additives (such as Mg^{2+} and Ca^{2+}).[31] However, the mechanisms of why and how the binary cation matrix benefits SEI stability are not fully understood. A significant barrier to investigate the intricate mechanisms that govern the SEI evolution during electrochemical cycling lies in the lack of *in situ* techniques that can capture SEI's dynamics and monitor its electronic and physical properties.

To bridge this knowledge gap, this work investigates the working mechanism of how multivalent cations stabilize the Si interface. Two distinct electrolyte environments are studied: (1) 0.2 M $Mg(TFSI)_2$ (magnesium bis(trifluoromethylsulfonyl)imide) in 1.2 M $LiPF_6$ (lithium hexafluorophosphate) in 3:7 wt% ethylene carbonate (EC) and ethyl methyl carbonate (EMC) with 10 wt% fluoroethylene carbonate, referred as the Mg^{2+}+Li^+ ion matrix electrolyte; (2) 1.2 M $LiPF_6$ (lithium hexafluorophosphate) in 3:7 wt% ethylene carbonate (EC) and ethyl methyl carbonate (EMC) with 10 wt% fluoroethylene carbonate, referred as the solely Li^+ electrolyte. Findings directly distinguish the gravimetric contribution at the Si interface from two distinct electrolyte environments, with insights into the SEI formation mechanism and the corresponding change of the viscoelastic properties at the interface. Results reveal that Mg^{2+} suppresses SEI gravimetrically by 70% before lithiation due to its preferred coordination with the EC solvent. The presence of Mg ions leads to an approximately 80% reduction in the post-Li SEI growth ascribed to the structural stabilization and the elimination of the complex Li_xSi_y phase formation that was unexplored previously. The presence of Mg ions contributes to the development of a more rigid and homogeneous SEI, as indicated by the reduced dissipation factor (ΔD) in the Mg^{2+}+Li^+ ion matrix compared to the solely Li^+ system. These findings contribute to a deep understanding of SEI dynamics and serve as a foundation for future research directed at developing strategies to enhance the performance and stability of Si anodes.

2. EXPERIMENTAL SECTION

2.1. Electrode and Electrolyte Preparation.

Si thin film electrodes were deposited onto 5 MHz Au-Ti AT-cut quartz crystal resonators (Q-Sense, Biolin Scientific, Sweden) and Cu foil (9 μm in thickness) by magnetron sputter

deposition (AJA International) with a DC power supply using an elemental Si (99.999%) target (Kurt J. Lesker, USA). A preliminary thin layer of Cu was sputtered onto both the quartz resonator and Cu foil substrates from the Cu target (99.999%, Kurt J. Lesker, USA), resulting in an approximate layer thickness of ~15 nm. Si-thin films with ~65 nm in thickness were obtained at a deposition rate of 4.129 nm/min. The base and working pressure of the deposition chamber were 2.6×10^{-7} Torr and 3 mTorr, respectively. Following the deposition procedure, the samples were promptly transferred to an Ar-filled glove box (Vacuum Technology Inc.), which maintained a controlled environment with H_2O and $O_2 < 0.1$ ppm. The solely Li^+ electrolyte consisted of 1.2 M lithium hexafluorophosphate ($LiPF_6$) in 3:7 wt% ethylene carbonate (EC) and ethyl methyl carbonate (EMC) and used as received (Tomiyama Chemicals, Japan) with 10 wt% fluoroethylene carbonate (FEC, Sigma Aldrich). Magnesium bis(trifluoromethylsulfonyl)imide (($Mg(TFSI)_2$, Solvionic, 99.5%) was dried overnight (at 180 °C, <100 mTorr) in a vacuum oven (Glass Oven B-585, BUCHI Corp.). The Mg^{2+}+Li^+ ion matrix electrolyte was prepared by adding $Mg(TFSI)_2$ salt into the fresh Li^+ electrolyte with a 10 wt% FEC to obtain 0.2 M $Mg(TFSI)_2$ concentration. The Fourier transform infrared (FTIR) spectra of the as-prepared electrolytes were collected using Nicolet iS50 FTIR spectrometer equipped with an attenuated total reflectance (ATR) detector at 32 scans with a spectral resolution of 4 cm^{-1} in the range between 4000–400 cm^{-1}.

2.2. EQCM-D and Electrochemistry Measurements.

Electrochemical quartz crystal microbalance measurements were carried out with a Q-sense instrument (Biolin Scientific, Sweden) located in the Ar-filled glovebox (Vacuum Technology Inc.) with H_2O and $O_2 < 0.1$ ppm. The measurements were conducted using an in-house designed electrochemical cell combined with an EQCM-D module. The EQCM-D resonators used in this work were AT-cut quartz crystals with an area of 0.785 cm^2 and a fundamental resonance frequency of 5 MHz. The Si thin film-coated EQCM-D resonator was used as a working electrode (WE) with lithium metal (99.9%, Goodfellow) as both reference (RE) and counter (CE) electrode. After the electrolyte was introduced into the EQCM-D cell, the baseline frequency and dissipation were recorded before the start of cyclic voltammetry (CV) measurements. The CV was performed by applying the potential at 0.001 V/s from open circuit voltage (OCV) to different lithiation depths (vs Li/Li^+) controlled by the Potentiostat (Princeton Applied Instruments). EQCM-D measurements were recorded at odd overtones (n = 3, 5, 7) using QSoft401 software. Data acquisition for the electrochemical measurements was performed using Versa Studio.

2.3. EIS Measurement and Fitting.

The electrochemical impedance spectroscopy (EIS) measurements were conducted using a Potentiostat (Princeton Applied Instruments) at room temperature. EIS was measured in a 2-electrode Swagelok cell with Si thin film as WE and Li metal as RE and CE. For EIS analysis, cells were held at a controlled discharge process where the potential was scanned from the OCV to specific voltage points at a scan rate of 0.001 V/s. The frequency range for EIS was set from 0.05 Hz to 1 MHz with an AC voltage amplitude of 10 mV. The EIS experimental data were fitted to the equivalent Randles circuit model using the AfterMath software (Pine Research Instrumentation, Durham, NC). The experimental EIS data was fitted to the equivalent circuit model consisting of the electronic elements of electrolyte resistance (R_s), charge transfer resistance (R_{ct}), constant phase element (Q_{CPE}), and Warburg component (Q_W).

3. RESULTS AND DISCUSSION

3.1. Mg Ion and its Effect on the Initial SEI Formation on Si.

Two electrolyte environments, (1) the Mg^{2+}+Li^+ ion matrix electrolyte and (2) the solely Li^+ electrolyte, were used on a carbon-free, binder-free, thin film Si anode. The in-situ SEI formation and evolution of the Si interface are distinguished and discussed at two electrochemical stages: Section 3.1.1 – the pre-lithiation (pre-Li*)* SEI stage, and Section 3.1.2 – the post-lithiation (post-Li) SEI stage.

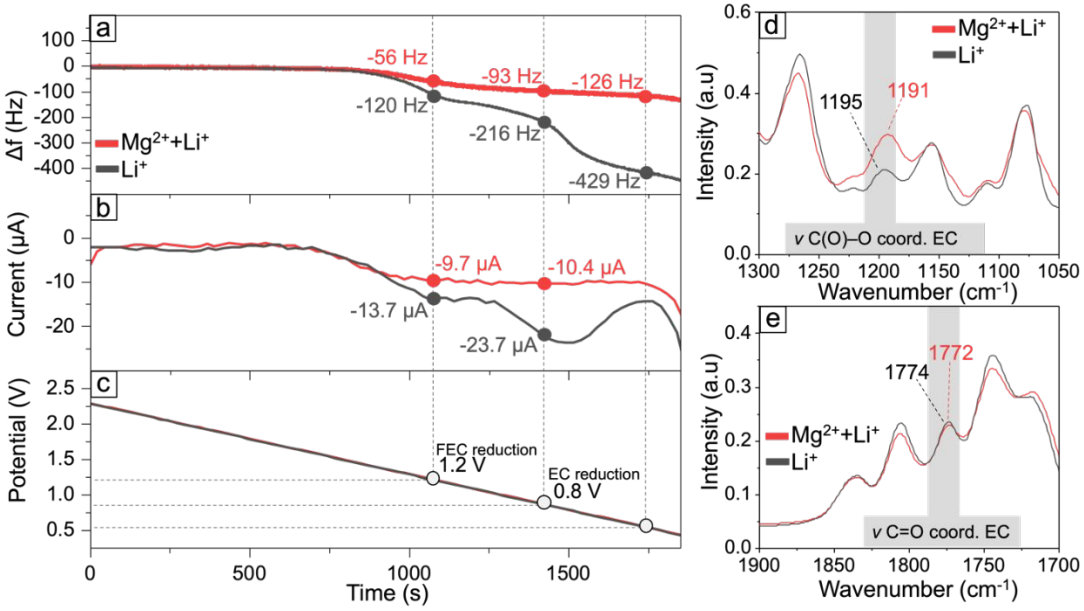

Figure 1. (a) Frequency change (Δf, n = 3) versus time at Si in the Mg^{2+}+Li^+ ion matrix (red) and solely Li^+ (black) electrolytes in the pre-Li stage (OCV – 0.5 V) of the 1st electrochemical cycle (CV # 1); (b) The corresponding current versus time and (c) potential versus time for Mg^{2+}+Li^+ ion matrix and solely Li^+. Si-coated resonator is used as WE, with Li metal as CE and RE, the cell is scanned at a potential window from OCV to 0.01 V at a scan rate of 1 mVs^{-1}. Frequency is taken at the 3rd overtone (n = 3). (d-e) FTIR spectra of Mg^{2+}+Li^+ ion matrix (red) and solely Li^+ (black) electrolytes.

3.1.1. Pre-Lithiation SEI on Si in an Ion Matrix of Mg^{2+}+Li^+.

The presence of Mg ions notably suppressed the SEI formation at initial electrochemical cycles before lithiation occurred. For instance, at the pre-Li stage from OCV to 0.5 V (**Figure 1a-c**), SEI formation in the Mg^{2+}+Li^+ ion matrix electrolyte was gravimetrically suppressed at voltages where solvent reduction typically occurred (1.2 V, 0.8 V, 0.5 V vs Li^+/Li). The total frequency drop Δf_{total} measured for the pre-Li voltages (OCV to 0.5 V) was 126 Hz in the Mg^{2+}+Li^+ ion matrix, as compared to 429 Hz in a solely Li^+ system (**Figure 1a).** Specifically, a one-step frequency change of ~ 56 Hz was seen in the Mg^{2+}+Li^+ ion matrix corresponding to the FEC reduction at 1.2 V (red curve in **Figure 1a**), while an evident two-step frequency change of 120 Hz and 216 Hz for the FEC and EC reductions was observed in the solely Li^+ electrolyte, respectively (black curve in **Figure 1a**). In agreement with the frequency changes, the corresponding current signals in the Mg^{2+}+Li^+ ion matrix were suppressed as compared to the

solely Li^+ system (**Figure 1b**). A flat current plateau of ~ -10 µA was seen throughout the pre-Li voltages in the Mg^{2+}+Li^+ ion matrix, and such plateau was mainly contributed by the FEC reduction.[33] While two discernible current peaks of -13.7 µA at 1.2 V for FEC reduction, and -23.7 µA at 0.8 V for EC reduction were seen in the solely Li^+ electrolyte system.[34] The mass-contributed SEI changes at the Si interface due to FEC and EC reductions were clearly distinguished by the frequency changes from the EQCM-D and indicated that introduction of Mg^{2+} into the Li^+ electrolyte plays a crucial role in the initial SEI suppression. Findings demonstrate that Mg^{2+} suppresses primary EC reduction specifically at the pre-Li stage at the initial CV cycle. The role of EC in the SEI formation and its function in electrolyte are critical since initial SEI acts as a protective and stabilizing layer for Si against further interfacial side reactions during subsequent electrochemical cycling.[35] Such a finding is further supported by the ex-situ XPS analysis investigating the postmortem SEI chemical structure, revealing a notable decrease in carbonate species with Mg^{2+} additives.[31]

To further explore possible mechanisms that led to the reduced EC solvent decomposition, the FTIR spectra of two electrolytes, the mixed cation of Mg^{2+}+Li^+ ion matrix and the solely Li^+ electrolyte, were compared. The interaction of the EC with the Mg^{2+} center was evident from the FTIR spectra (**Figure 1d-e**) for the uncycled Mg^{2+}+Li^+ ion matrix versus the solely Li^+ electrolyte. The noticeable shifts to lower wavenumbers in the positions of the C═O peak and the C(O)-C peak of coordinated EC were seen, indicating coordination of EC with the Mg ions.[36] The changes in the coordination environment alter the electronic properties of solvent molecules and can increase the energy barriers for solvent reduction, ultimately resulting in a decrease in solvent reductivity.[37, 38] Elimination of the EC solvent reduction is essentially attributed to the coordination of the EC-Mg^{2+} that fundamentally decreases the electrochemical reduction of EC. It is worth noting that the lack of noticeable reduction currents in the subsequent CV cycles (**Figure S1, SI**) emphasizes that the primary formation of SEI occurs during the initial CV cycle. However, this observation does not rule out the possibility of continuous SEI formation beyond the pre-Li stage.

3.1.2. SEI Retention at the Post-Lithiation Stage and its Evolution.

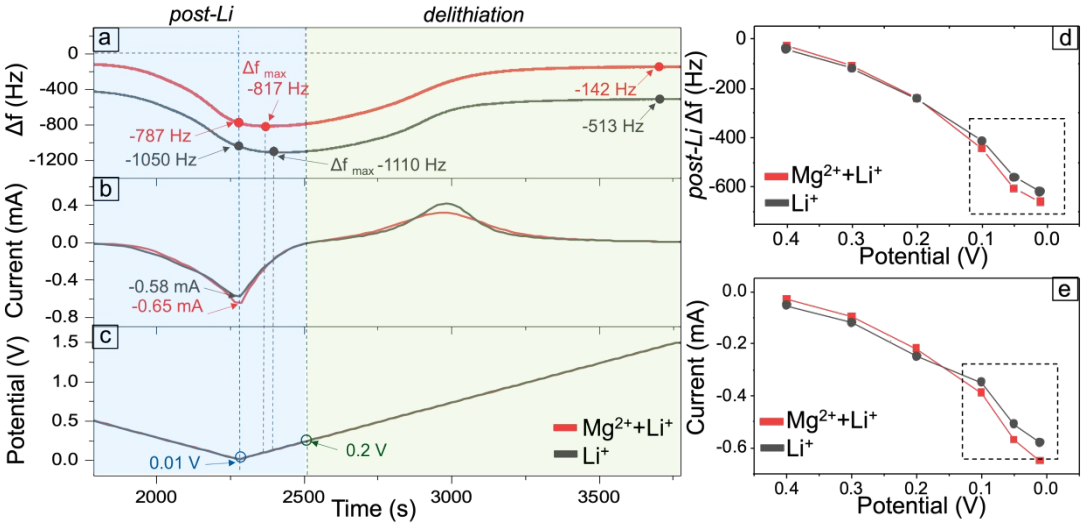

Figure 2. (a) The change of frequency (Δf, n = 3) versus time at Si in the Mg^{2+}+Li^+ ion matrix (red) and a solely Li^+ electrolyte (black) in the post-Li stage (< 0.5 V) and delithiation stage (0.2

V – 1.5 V), data taken at the 1st electrochemical cycle (CV #1); (b) The corresponding current versus time and (c) potential versus time. (d) The change of frequency (Δf, n = 3) versus potential, and € the corresponding current versus potential, ascribed to the post-Li stage. Si-coated resonator is used as WE, with Li metal as CE and RE, potential is scanned from OCV to 0.01 V at a scan rate of 1 mVs^{-1}. Frequency is taken at the 3rd overtone (n = 3).

In the post-Li stage, with voltage from 0.5 V to 0.01 V (vs Li/Li^+) (**Figure 2**), one of the most interesting findings was that the SEI continuously developed during lithiation as indicated in **Figure 2a**. However, post-Li the SEI was gravimetrically less significant than the pre-Li SEI, and it merely constituted less than 20 % when gravimetrically referenced to the pre-Li SEI. For instance, the SEI formation at the post-Li stage (0.5 V to 0.01 V) presented a Δf of 16 Hz in the Mg^{2+}+Li^+ ion matrix and 84 Hz in the solely Li^+ electrolyte. In contrast with the pre-Li SEI formation of 126 Hz in the Mg^{2+}+Li^+, and 429 Hz in the solely Li^+ electrolyte. Nonetheless, the addition of Mg noticeably reduced the post-Li SEI by about 80% gravimetrically due to the continuous suppression of the electrolyte reduction that consequently led to reduced reactivity of lithiated Si, which contributes to the overall improved SEI stability.

At deep lithiation stage from 0.1 V to 0.01 V (vs Li/Li^+), Mg ion facilitated a co-insertion or an ion exchange reaction that resulted in a greater change of current and frequency as suggested by the highlighted frequency versus voltage regions in **Figure 2d-e**.[27, 32] Thus, the Mg ion helped to stabilize the lithiated silicide surface. The total frequency and current changes ascribed to the post-Li stage suggested that the largest frequency discrepancy in the Mg^{2+}+Li^+ ion matrix versus the solely Li^+ system appeared at deeper lithiation of 0.1 V and beyond (highlighted in the dashed area in **Figure 2d**). The observed maximum frequency change (Δf_{max}) did not coincide with the peak current as seen in **Figure 2a**. Instead, the Δf_{max} was detected at higher voltages during the reverse voltage scan, suggesting that alloying processes continued past the peak current. For the mixed Mg^{2+}+Li^+ ion matrix, the Δf_{max} occurred at a reverse voltage scan of +0.07 V, while for the solely Li^+ system, the peak frequency change was observed at +0.11 V. Such ongoing lithiation is likely a result of the reactions involving Si that has been exposed and expanded during the deep lithiation phase. For instance, at a lithiation voltage of 0.01 V, additional frequency shifts of 30 Hz for Mg^{2+}+Li^+ ion matrix and 60 Hz for solely Li^+ were observed which suggests that the presence of Mg^{2+} exerts a stabilizing effect on the lithiated silicon framework. The multifold combination of EQCM-D with electrochemistry in situ probing revealed intricate links between Si reactivity and the electrochemical processes at the interface.

After completion of the 1st electrochemical cycle, and upon delithiation, from 0.2 V to 1.5 V **(Fig. 2**, green-colored block), the frequency baseline did not revert to its initial baseline of 0 Hz, and a notable frequency shift was observed, 142 Hz for Mg^{2+}+Li^+ ion matrix and 513 Hz for solely Li^+ electrolyte. This shift signifies that the presence of SEI persists at the Si interface upon delithiation or with the completion of the electrochemical cycles. Such an SEI layer was gravimetrically 4 times lower in the Mg^{2+}+Li^+ ion matrix vs solely Li^+ electrolyte. The SEI retention upon delithiation is ascribed to either further reduction of electrolyte concurrent with Li dealloying or the existence of ions irreversibly trapped within the Si structure during the dealloying process.[39]

3.2. Lithiation Depth to SEI Evolution of Si in Solely Li^+ or Mixed Mg^{2+}+Li^+ Electrolytes.

The SEI growth and stability are closely linked to Si volume expansion, with this relationship becoming especially critical at the deep lithiation stage. To comprehensively explore the impact of lithiation depth versus the electrochemical cycles on SEI evolution, a set of four consecutive CV scans was collected at different lithiation depths for a total of 20 CV cycles (**Figure 3**). CV # 1 - 4 correspond to a lithiation depth of 0.01 V, CV # 5 – 8 to a depth of 0.04 V, CV # 9 – 12 to a depth of 0.115 V, CV # 13-16 to a depth of 0.4 V, and CV # 17 - 20 correspond to lithiation depth of 0.005 V.

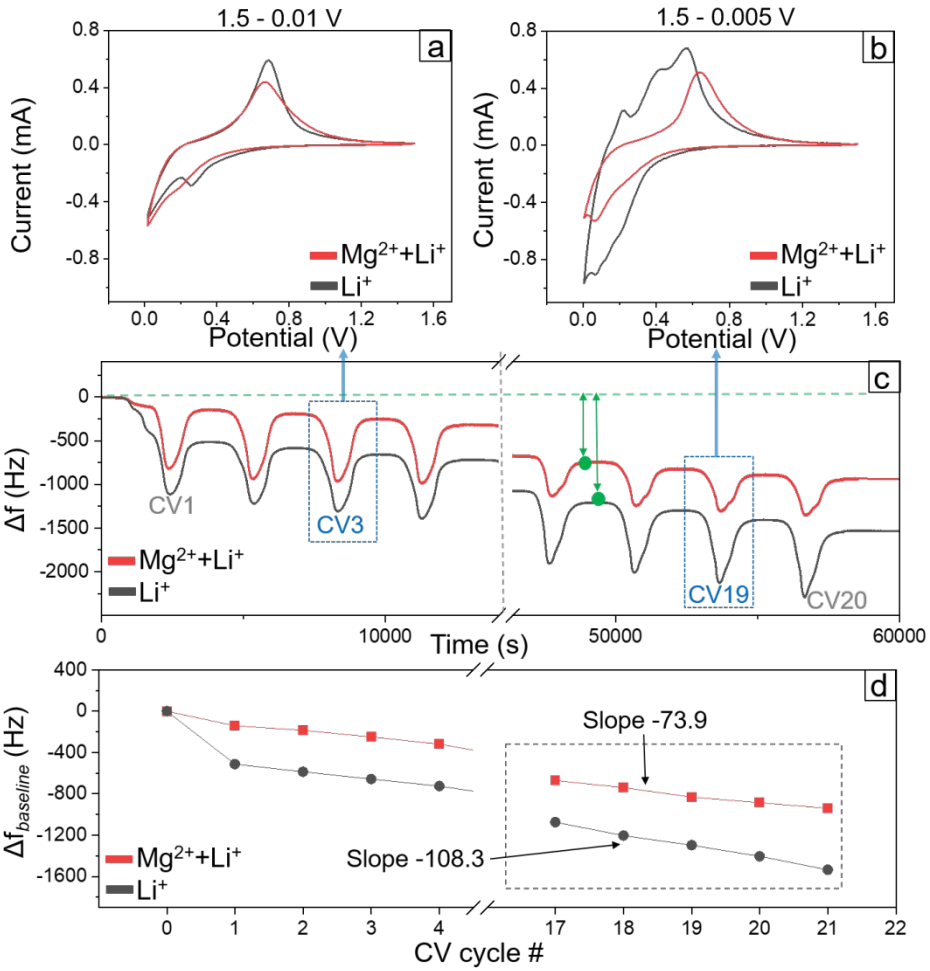

Figure 3. Cyclic Voltammetry of Si thin film anode vs Li at lithiation depth of (a) 0.01 V and (b) 0.005 V at continuous CV cycles (3rd CV cycle is used as the representative).; (c) Frequency change (Δf, n = 3) at corresponding lithiation depths, the dashed green line indicates the frequency baseline, and the grey vertical dashed lines separate each set of four CVs collected at different lithiation depths; (d) Frequency baseline shift ($\Delta f_{baseline}$) versus cycle number. Red and black curves stand for Mg^{2+}+Li^+ ion matrix electrolyte and solely Li^+ electrolyte, respectively. PVD sputtered Si thin film resonator is used as WE, Li metal is used as CE and RE. Cell is scanned at a potential window from OCV to 0.01 V at a scan rate of 1 mVs^{-1}. Frequency is taken at the 3rd overtone (n = 3).

The CVs at two representative lithiation depths of 0.01 V and 0.005 V for Mg^{2+}+Li^+ ion matrix and solely Li^+ electrolyte systems are presented in **Figure 3a-b**. The addition of Mg ions to the Li electrolyte suppressed the formation of complex Li-Si phases especially pronounced at the deep lithiation stage. At the lithiation depth of 0.01 V, **Figure 3a,** the Mg^{2+}+Li^+ ion matrix CV (red) presented the absence of the characteristic reduction peak in the solely Li^+ system at ~0.3 V for alloying of Li with amorphous Si (*a*Si+Li → *a*SiLi) (black).[40, 41] However, a shifted reduction peak at 0.007 V was seen for the formation of the *a*SiLi at a lithiation depth of 0.005 V in the Mg^{2+}+Li^+ ion matrix electrolyte (**Figure 3b**). Such voltage shift has been previously observed in the lithiation of binary Si/Ni thin film wherein the inactive Ni during lithiation caused a suppression of the lithiation voltage.[42] Possible formation of the Li-Mg-Si ternary phase can potentially suppress such formation of *c*$Li_{15}Si_4$, and this phenomenon has also been verified in the electrochemical formation of Li-Zn-Si ternaries where *c*$Li_{15}Si_4$ phase formation was suppressed resulting in full amorphization of the Si film.[43] Additionally, the absence of the redox peaks in the Mg^{2+}+Li^+ ion matrix was evident in CVs at lithiation depths of 0.04 V and 0.115 V (**Figure S2, SI**). In contrast, in a solely Li^+ electrolyte system, a broad lithiation peak at 0.3 V for *a*SiLi was seen at lithiation depth of 0.005 V (**Figure 3b**) followed by a second peak below 0.01 V indicating the formation of a metastable *c*$Li_{15}Si_4$ phase upon further Li alloying (*a*SiLi + Li → *c*$Li_{15}Si_4$).[44, 45]

Figure 3c-d summarizes the shift of the baseline frequency ($\Delta f_{baseline}$) at lithiation depth at 0.01 V and 0.005 V in the Mg^{2+}+Li^+ ion matrix (red) vs solely Li^+ system (black). At lithiation depth of 0.005 V, a continuous increase in SEI growth was observed, driven by Si expansion and exposure of fresh Si, making the interface susceptible to potential surface side reactions. This continuous SEI growth contributes to a loss of lithium-ion inventory, leading to a capacity fade. The Mg^{2+}+Li^+ ion matrix exhibited a suppressed SEI growth indicating enhanced surface stability as highlighted by the smaller baseline frequency shift (slope of 73.9) compared to the solely Li^+ electrolyte (slope of 108.3) shown in **Figure 3d** (dashed box). Results suggest the Mg^{2+} induced structural stabilization in the lithiated Si, suppressing side reactions, and promoting controlled SEI growth. The formation of a Li-Mg-Si ternary phase is responsible for this effect, introducing amorphization in the Si structure and preventing the crystalline $Li_{15}Si_4$ phase. This is crucial, as amorphous Si is known for outperforming its crystalline counterpart due to enhanced mechanical stability in the film.[46-48]

3.3. Electrochemical Impedance Spectroscopy at Pre-Lithiation vs Post-Lithiation of Si in the Mg^{2+}+Li^+ and Li^+ Electrolytes.

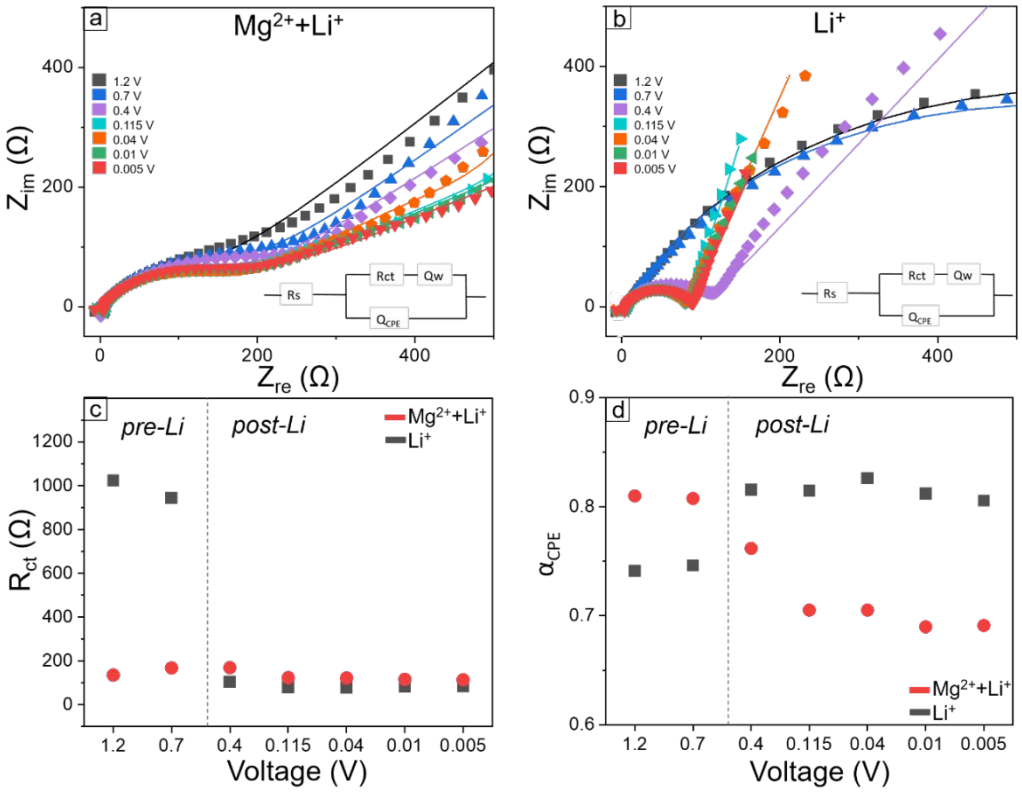

Figure 4. Nyquist plots for thin film Si anode vs Li in (a) Mg^{2+}+Li^+ ion matrix and (b) solely Li^+ electrolytes, at different lithiation voltages. Pre-Li stage at 1.2 V, 0.7 V, and post-Li stage at 0.4 V, 0.115 V, 0.04 V, 0.01 V and 0.005 V are investigated; Symbols represent experimental data points, while lines depict fitted data obtained from the equivalent circuit model. EIS was measured in the 2-electrode Swagelok cell with Si thin film as WE and Li metal as RE/CE by sequential voltage scan at a scan rate of 0.001 V/s from OCV to the target voltage followed by EIS measurement. (c) R_{ct} vs lithiation depths, and (d) α_{CPE} vs lithiation depths.

Results from EIS demonstrated a substantial tenfold decrease in the charge transfer resistance (R_{ct}) for Si in the Mg^{2+}+Li^+ ion matrix electrolyte before lithiation occurred as compared with the solely Li^+ electrolyte, R_{ct} dropped from 1000 ohms (in the solely Li^+ system) to 150 ohms at lithiation depth of 1.2 V (pre-Li) and 0.7 V (pre-Li) in **Figure 4a-c** (complete Nyquist plots and fitted data are presented in **Figure S3 and Table S1, SI)**. In line with findings from EQCM-D and FTIR, such a decrease in R_{ct} directly indicates improved charge transfer kinetics attributed to Mg^{2+} presence in the electrolyte, linked to the formation of MgF_2 at the interface.[49, 50] On the other hand, the solely Li^+ system resulted in the formation of SEI-rich interphase with species from FEC and EC reduction such as lithium carbonate (Li_2CO_3) and lithium alkyl carbonate ($ROCO_2Li$) giving rise to the increased R_{ct}.[51]

As lithiation progressed (from 0.7 V to 0.4 V, 0.115 V, 0.04 V, 0.01 V and 0.005 V), a general decline in the total impedance was seen concurrently for Si in both the Mg^{2+}+Li^+ ion matrix and the solely Li^+ systems ascribed to an increase in the total electronic conductivity of Si.[52] Q_{CPE} is related to the magnitude of the capacitance, and an exponent α_{CPE} which reflects the deviation from the ideal capacitive behavior at the electrochemical interfaces.[53] The increase in α_{CPE} was

observed with the increase in lithiation depth for the Li^+ system in **Figure 4d** indicating a more ideal capacitive behavior, potentially due to an enhanced surface roughness that homogenizes the electrochemical properties across the electrode, suggesting rougher surfaces promote closer-to-ideal capacitance.[54] In contrast, the Mg^{2+}+Li^+ system showed the decrease in α_{CPE} indicates a deviation from ideal capacitance due to modification of surface characteristics by Mg^{2+} addition, thus leading to a less capacitive and more resistive behavior as reflected by a lower α_{CPE}.[54, 55] The reduced α_{CPE} in the Mg^{2+}+Li^+ implies a more uniform and possibly smoother interface on lithiated Si, which is indicative of a stabilized interphase that comes along with a reduced SEI formation observed from EQCM-D results (**Figures 1-2**). The phase angle of Warburg diffusion for the Mg^{2+}+Li^+ system was decreased from 45° to 25° at increased lithiation depth suggesting the resistance-dominated finite length Warburg, on the contrary, it was increased from 45° (1.2 V) to 73° (at 0.005 V) for the solely Li^+ system. This suggests that Mg^{2+} addition induced deviation from a semi-infinite diffusion model to a finite boundary Warburg.[54, 56, 57] Further, the Bode plots suggested a less frequency dependence for the phase angle at lithiation in the Mg^{2+}+Li^+ ion matrix against the Li^+ system (**Figure S4, SI**). This suggests that the Mg^{2+}+Li^+ ion matrix displays a more linear response in the low-frequency range in contrast with the solely Li^+ system.

3.4. Viscoelastic Properties at Si Interphase in a Binary Mg^2+Li^+ Ion Matrix Versus Solely Li^+ System at Si.

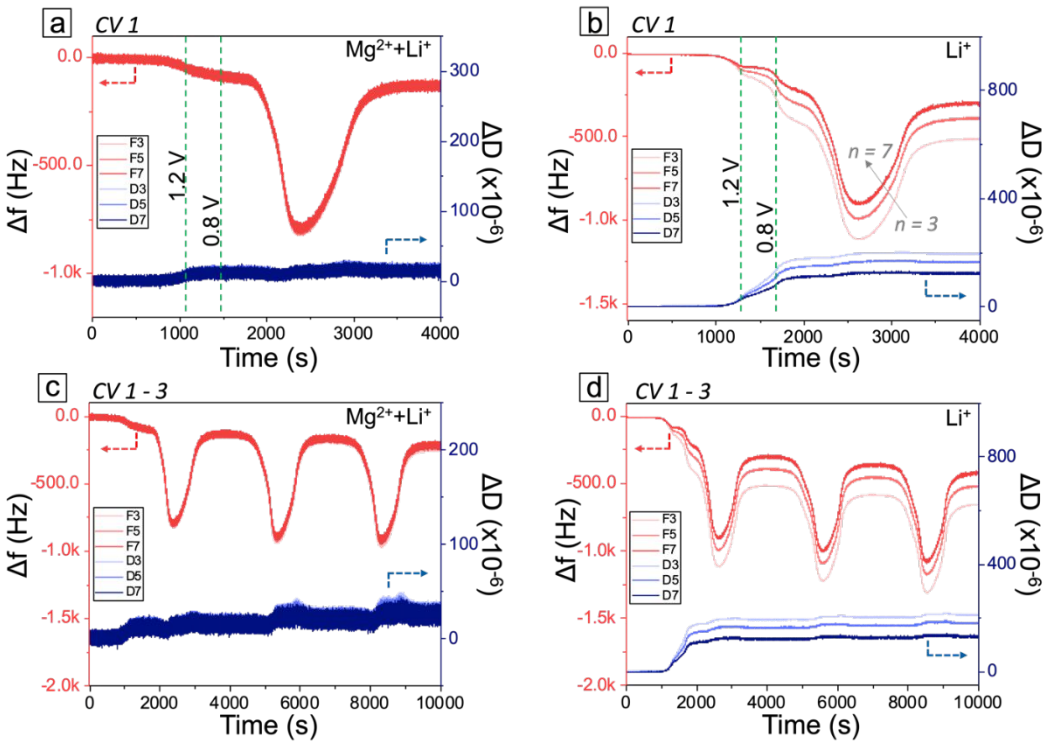

Figure 5. Dissipation (ΔD) of EQCM-D over time at n = 3, 5, 7 for (a, c) in the Mg^{2+}+Li^+ ion matrix electrolyte (CV#1 for panel a, CV#1-3 for panel c) and (b, d) in a solely Li^+ electrolyte (CV#1 for panel b, CV#1-3 for panel d).

Development of a notably more rigid SEI in the Mg^{2+}+Li^+ ion matrix is seen at initial CV cycle as reflected by a significantly reduced dissipation shift when compared to the solely Li^+ system, shown in **Figure 5a-b**. Introducing Mg ions led to a fourfold reduction in ΔD compared to the solely Li^+ system. This finding suggests two key insights: (1) a more homogeneous SEI evolution is seen across the interphase in the Mg^{2+}+Li^+ ion matrix as demonstrated by the lower spreading of ΔD values at different harmonics (n = 3, 5, 7); (2) SEI displays minimal energy loss and enhances structural stability in the Mg^{2+}+Li^+ ion matrix, resulting in a more uniform and rigid interface with reduced detachment from the underlying Si which supports a reduced α_{CPE} in the presence of Mg^{2+} suggested from the EIS findings in **Figure 4d**.[58]

A detailed analysis of ΔD at the initial CV cycle and further continuous CVs was investigated. With the introduction of Mg^{2+}, ΔD shift was five times smaller compared to the solely Li^+ electrolyte in the pre-Li stage (**Figure 5a**), suggesting formation of a notably more rigid SEI. The suppressed FEC and EC reductions result in a more rigid and mechanically stable interphase. This finding is supported by a recent work where XPS analysis revealed an inorganic SEI of MgF_2, MgO, and $MgCO_3$-rich layer with the presence of Mg^{2+}.[31] In contrast, the solely Li^+ system followed a well-reported two-layer SEI model where the initial inorganic-rich SEI is formed and followed by the outer organic-rich layer.[59-61] The initial ΔD increase at ~1.2 V is attributed to FEC reduction and the inorganic SEI layer formation as supported by the experimental data in **Figure 5b**, followed by a significant ΔD increase at 0.8 V for EC reduction, generating organic compounds which predominantly contributed to the increase in viscoelastic properties at the interface. After three CV cycles (**Figure 5c-d**), the ΔD values for the solely Li^+ system (~200×10^{-6}, n = 3) were nearly four times greater than those for the Mg^{2+}+Li^+ system (~50×10^{-6}, n = 3), at comparable frequency and current changes. This indicates that the SEI in the Mg^{2+}+Li^+ ion matrix is considerably more rigid and is homogeneously distributed across the interface than in the solely Li^+ electrolyte. The Mg^{2+}+Li^+ ion matrix offered a more robust and uniform SEI layer compared to the Li^+ system. Such enhanced rigidity contributes to mechanical stability, reducing the risk of Si cracking during cycles and improving overall electrode durability, and preserving the electrode's integrity.

4. CONCLUSIONS

This study highlights the significant role of a binary cation electrolyte with the presence of Mg ion that reduces SEI growth before and after lithiation for a Si anode. The binary cation matrix of the Mg^{2+}+Li^+ electrolyte altered the solvation structure of the Li^+ environment, resulting in a distinct SEI formation mechanism. The initial SEI formation before lithiation is reduced by 70% in the binary Mg^{2+}+Li^+ electrolyte. While the post-lithiation SEI growth is suppressed by about 80% with the presence of Mg^{2+} in electrolyte and a reduced activity of lithiated Si is seen along with a rigid and homogeneous SEI formation. Results from this work offer insights into SEI dynamics and pave the way for designing more robust Si electrodes for next-generation lithium-ion batteries.

ASSOCIATED CONTENT

Supporting Information

Supporting information is available free of charge online. Additional electrochemical CV cycles, Nyquist plots and Bode plots are presented in SI.

AUTHOR INFORMATION

Corresponding Author
Niya Sa – *Department of Chemistry, University of Massachusetts – Boston, Boston, Massachusetts 02125, United States;*
Email: Niya.Sa@umb.edu

Authors
Saida Cora - *Department of Chemistry, University of Massachusetts – Boston, Boston, Massachusetts 02125, United States;*
Zicheng Yang - *Department of Chemistry, University of Massachusetts – Boston, Boston, Massachusetts 02125, United States.*
John T. Vaughey - *Chemical Sciences and Engineering Division, Agonne National Laboratory, Lemonyt, IL, 60439 United States*

ACKNOWLEDGMENTS

This work is primarily financially supported by the NSF CAREER grant (Grant No. 2047753). Acquisition of the advanced FESEM is acknowledged from the MRI grant of the National Science Foundation (Grant No. 1919919). The US Department of Energy (DOE)'s Vehicle Technologies Office under the Silicon Consortium Project is acknowledged. This work was conducted in part by UChicago Argonne, LLC, Operator of Argonne National Laboratory ('Argonne'). Argonne, a US DOE Office of Science laboratory, is operated under contract no. DE-AC02-06CH11357. Author Saida Cora is partially sponsored by the U.S. Department of Energy, Office of Science, Office of Workforce Development for Teachers and Scientists, Office of Science Graduate Student Research (SCGSR) program. The SCGSR program is administered by the Oak Ridge Institute for Science and Education (ORISE) for the DOE. ORISE is managed by ORAU under contract number DE-SC0014664. The US Government retains and the publisher, by accepting the article for publication, acknowledges that the US Government retains a non-exclusive, paid-up, irrevocable, worldwide license to publish or reproduce the published form of this work, or allow others to do so, for US Government purposes. All opinions expressed in this paper are the author's and do not necessarily reflect the policies and views of DOE, ORAU, or ORISE. N.S. would also like to thank Steve Shepard and his support with the cleanroom of the Boston College Integrated Sciences.

REFERENCES

(1) Duan, J.; Tang, X.; Dai, H. F.; Yang, Y.; Wu, W. Y.; Wei, X. Z.; Huang, Y. H., Building Safe Lithium-Ion Batteries for Electric Vehicles: A Review. *Electrochem. Energy R* **2020,** *3* (1), 1-42.
(2) Zubi, G.; Dufo-López, R.; Carvalho, M.; Pasaoglu, G., The lithium-ion battery: State of the art and future perspectives. *Renew. Sust. Energ. Rev.* **2018,** *89*, 292-308.

(3) Kim, T.; Song, W. T.; Son, D. Y.; Ono, L. K.; Qi, Y. B., Lithium-ion batteries: outlook on present, future, and hybridized technologies. *J. Mater. Chem. A* **2019,** *7* (7), 2942-2964.
(4) Wulandari, T.; Fawcett, D.; Majumder, S. B.; Poinern, G. E. J., Lithium-based batteries, history, current status, challenges, and future perspectives. *Battery Energy* **2023,** *2* (6), 20230030.
(5) Li, M.; Lu, J.; Chen, Z. W.; Amine, K., 30 Years of Lithium-Ion Batteries. *Adv. Mater.* **2018,** *30* (33), 1800561.
(6) Blomgren, G. E., The Development and Future of Lithium Ion Batteries. *J. Electrochem. Soc.* **2017,** *164* (1), A5019-A5025.
(7) Nitta, N.; Wu, F. X.; Lee, J. T.; Yushin, G., Li-ion battery materials: present and future. *Mater. Today* **2015,** *18* (5), 252-264.
(8) Obrovac, M. N.; Chevrier, V. L., Alloy Negative Electrodes for Li-Ion Batteries. *Chem. Rev.* **2014,** *114* (23), 11444-11502.
(9) Zhang, W. J., A review of the electrochemical performance of alloy anodes for lithium-ion batteries. *J. Power Sources* **2011,** *196* (1), 13-24.
(10) Liang, C.; Gao, M. X.; Pan, H. G.; Liu, Y. F.; Yan, M., Lithium alloys and metal oxides as high-capacity anode materials for lithium-ion batteries. *J. Alloy Compd.* **2013,** *575*, 246-256.
(11) Sun, L.; Liu, Y. X.; Shao, R.; Wu, J.; Jiang, R. Y.; Jin, Z., Recent progress and future perspective on practical silicon anode-based lithium ion batteries. *Energy Storage Mater.* **2022,** *46*, 482-502.
(12) Gonzalez, A. F.; Yang, N. H.; Liu, R. S., Silicon Anode Design for Lithium-Ion Batteries: Progress and Perspectives. *J. Phys. Chem. C* **2017,** *121* (50), 27775-27787.
(13) Feng, K.; Li, M.; Liu, W. W.; Kashkooli, A. G.; Xiao, X. C.; Cai, M.; Chen, Z. W., Silicon-Based Anodes for Lithium-Ion Batteries: From Fundamentals to Practical Applications. *Small* **2018,** *14* (8), 1702737.
(14) Zuo, X. X.; Zhu, J.; Müller-Buschbaum, P.; Cheng, Y. J., Silicon based lithium-ion battery anodes: A chronicle perspective review. *Nano Energy* **2017,** *31*, 113-143.
(15) Li, F. R.; Xu, J.; Hou, Z. W.; Li, M.; Yang, R., Silicon Anodes for High-Performance Storage Devices: Structural Design, Material Compounding, Advances in Electrolytes and Binders. *ChemNanoMat.* **2020,** *6* (5), 720-738.
(16) Eshetu, G. G.; Figgemeier, E., Confronting the Challenges of Next-Generation Silicon Anode-Based Lithium-Ion Batteries: Role of Designer Electrolyte Additives and Polymeric Binders. *ChemSusChem.* **2019,** *12* (12), 2515-2539.
(17) Yoon, T.; Nguyen, C. C.; Seo, D. M.; Lucht, B. L., Capacity Fading Mechanisms of Silicon Nanoparticle Negative Electrodes for Lithium Ion Batteries. *J. Electrochem. Soc.* **2015,** *162* (12), A2325-A2330.
(18) Li, T.; Yang, J. Y.; Lu, S. G.; Wang, H.; Ding, H. Y., Failure mechanism of bulk silicon anode electrodes for lithium-ion batteries. *Rare Metals* **2013,** *32* (3), 299-304.
(19) Shi, F. F.; Song, Z. C.; Ross, P. N.; Somorjai, G. A.; Ritchie, R. O.; Komvopoulos, K., Failure mechanisms of single-crystal silicon electrodes in lithium-ion batteries. *Nat. Commun.* **2016,** *7*, 11886.
(20) Yen, Y. C.; Chao, S. C.; Wu, H. C.; Wu, N. L., Study on Solid-Electrolyte-Interphase of Si and C-Coated Si Electrodes in Lithium Cells. *J. Electrochem. Soc.* **2009,** *156* (2), A95-A102.
(21) Chen, X.; Li, H. X.; Yan, Z. H.; Cheng, F. Y.; Chen, J., Structure design and mechanism analysis of silicon anode for lithium-ion batteries. *Sci. China Mater.* **2019,** *62* (11), 1515-1536.

(22) Li, L.; Fang, C.; Wei, W. F.; Zhang, L.; Ye, Z.; He, G.; Huang, Y. H., Nano-ordered structure regulation in delithiated Si anode triggered by homogeneous and stable Li-ion diffusion at the interface. *Nano Energy* **2020,** *72*, 104651.
(23) Jin, Y.; Li, S.; Kushima, A.; Zheng, X. Q.; Sun, Y. M.; Xie, J.; Sun, J.; Xue, W. J.; Zhou, G. M.; Wu, J.; Shi, F. F.; Zhang, R. F.; Zhu, Z.; So, K. P.; Cui, Y.; Li, J., Self-healing SEI enables full-cell cycling of a silicon-majority anode with a coulombic efficiency exceeding 99.9%. *Energy Environ. Sci.* **2017,** *10* (2), 580-592.
(24) Casimir, A.; Zhang, H. G.; Ogoke, O.; Amine, J. C.; Lu, J.; Wu, G., Silicon-based anodes for lithium-ion batteries: Effectiveness of materials synthesis and electrode preparation. *Nano Energy* **2016,** *27*, 359-376.
(25) Preman, A. N.; Lee, H.; Yoo, J.; Kim, I.; Saito, T.; Ahn, S. K., Progress of 3D network binders in silicon anodes for lithium ion batteries. *J. Mater. Chem. A* **2020,** *8* (48), 25548-25570.
(26) Markevich, E.; Salitra, G.; Aurbach, D., Fluoroethylene Carbonate as an Important Component for the Formation of an Effective Solid Electrolyte Interphase on Anodes and Cathodes for Advanced Li-Ion Batteries. *ACS Energy Lett.* **2017,** *2* (6), 1337-1345.
(27) Han, B. H.; Liao, C.; Dogan, F.; Trask, S. E.; Lapidus, S. H.; Vaughey, J. T.; Key, B., Using Mixed Salt Electrolytes to Stabilize Silicon Anodes for Lithium-Ion Batteries via in Situ Formation of Li-M-Si Ternaries (M = Mg, Zn, Al, Ca). *ACS Appl. Mater. Interfaces* **2019,** *11* (33), 29780-29790.
(28) Li, Z. F.; Stetson, C.; Teeter, G.; Norman, A.; Ha, Y. Y.; de Villers, B. J. T.; Huey, Z.; Walker, P.; Han, S. D.; DeCaluwe, S. C.; Jiang, C. S.; Burrell, A. K.; Zakutayev, A., Improving Interface Stability of Si Anodes by Mg Coating in Li-Ion Batteries. *ACS Appl. Energy Mater.* **2020,** *3* (12), 11534-11539.
(29) Baran, V.; van Wüllen, L.; Fässler, T. F., S Substitution of Lithium for Magnesium, Zinc, and Aluminum in $Li_{15}Si_4$: Crystal Structures, Thermodynamic Properties, as well as ^6Li and ^7Li NMR Spectroscopy of $Li_{15}Si_4$ and $Li_{15-x}M_xSi_4$ (M=Mg, Zn, and Al). *Chem. Eur. J.* 2016, *22* (19), 6598-6609.
(30) Zeilinger, M.; Baran, V.; van Wüllen, L.; Häussermann, U.; Fässler, T. F., Stabilizing the Phase $Li_{15}Si_4$ through Lithium–Aluminum Substitution in $Li_{15-x}Al_xSi_4$ ($0.4 < x < 0.8$)—Single Crystal X-ray Structure Determination of $Li_{15}Si_4$ and $Li_{14.37}Al_{0.63}Si_4$. *Chem. Mater.* 2013, *25* (20), 4113-4121.
(31) Yang, Z. Z.; Trask, S. E.; Gilbert, J. A.; Li, X.; Tsai, Y. F.; Jansen, A. N.; Ingram, B. J.; Bloom, I., Exploring the Promise of Multifunctional "Zintl-Phase-Forming" Electrolytes for Si-Based Full Cells. *ACS Appl. Mater. Interfaces* **2022,** *14* (48), 53860-53871.
(32) Li, X.; Gilbert, J. A.; Trask, S. E.; Uppuluri, R.; Lapidus, S. H.; Cora, S.; Sa, N. Y.; Yang, Z. Z.; Bloom, I. D.; Dogan, F.; Vaughey, J. T.; Key, B., Investigating Ternary Li-Mg-Si Zintl Phase Formation and Evolution for Si Anodes in Li-Ion Batteries with Mg(TFSI) Electrolyte Additive. *Chem. Mater.* **2021,** *33* (13), 4960-4970.
(33) Yao, K.; Zheng, J. P.; Liang, R., Ethylene carbonate-free fluoroethylene carbonate-based electrolyte works better for freestanding Si-based composite paper anodes for Li-ion batteries. *J. Power Sources* **2018,** *381*, 164-170.
(34) Veith, G. M.; Doucet, M.; Sacci, R. L.; Vacaliuc, B.; Baldwin, J. K.; Browning, J. F., Determination of the Solid Electrolyte Interphase Structure Grown on a Silicon Electrode Using a Fluoroethylene Carbonate Additive. *Sci. Rep.* **2017,** *7*, 6326.

(35) Vogl, U. S.; Lux, S. F.; Crumlin, E. J.; Liu, Z.; Terborg, L.; Winter, M.; Kostecki, R., The Mechanism of SEI Formation on a Single Crystal Si(100) Electrode. *J. Electrochem. Soc.* **2015,** *162* (4), A603-A607.
(36) Pekarek, R. T.; Affolter, A.; Baranowski, L. L.; Coyle, J.; Hou, T. Z.; Sivonxay, E.; Smith, B. A.; McAuliffe, R. D.; Persson, K. A.; Key, B.; Apblett, C.; Veith, G. M.; Neale, N. R., Intrinsic chemical reactivity of solid-electrolyte interphase components in silicon-lithium alloy anode batteries probed by FTIR spectroscopy. *J. Mater. Chem. A* **2020,** *8* (16), 7897-7906.
(37) Lautar, A. K.; Bitenc, J.; Rejec, T.; Dominko, R.; Filhol, J. S.; Doublet, M. L., Electrolyte Reactivity in the Double Layer in Mg Batteries: An Interface Potential-Dependent DFT Study. *J. Am. Chem. Soc.* **2020,** *142* (11), 5146-5153.
(38) Wang, C. Y.; Huang, Y.; Lu, Y. H.; Pan, H. G.; Xu, B. B.; Sun, W. P.; Yan, M.; Jiang, Y. Z., Reversible Magnesium Metal Anode Enabled by Cooperative Solvation/Surface Engineering in Carbonate Electrolytes. *Nano-Micro Lett.* **2021,** *13* (1), 195.
(39) Zhang, T.; Zhang, H. P.; Yang, L. C.; Wang, B.; Wu, Y. P.; Takamur, T., The structural evolution and lithiation behavior of vacuum-deposited Si film with high reversible capacity. *Electrochim. Acta* **2008,** *53* (18), 5660-5664.
(40) Fears, T. M.; Doucet, M.; Browning, J. F.; Baldwin, J. K. S.; Winiarz, J. G.; Kaiser, H.; Taub, H.; Sacci, R. L.; Veith, G. M., Evaluating the solid electrolyte interphase formed on silicon electrodes: a comparison of X-ray photoelectron spectroscopy and neutron reflectometry. *Phys. Chem. Chem. Phys.* **2016,** *18* (20), 13927-13940.
(41) Jerliu, B.; Hüger, E.; Dörrer, L.; Seidlhofer, B. K.; Steitz, R.; Horisberger, M.; Schmidt, H., Lithium insertion into silicon electrodes studied by cyclic voltammetry and neutron reflectometry. *Phys. Chem. Chem. Phys.* **2018,** *20* (36), 23480-23491.
(42) Du, Z. J.; Hatchard, T. D.; Dunlap, R. A.; Obrovac, M. N., Combinatorial Investigations of Ni-Si Negative Electrode Materials for Li-Ion Batteries. *J. Electrochem. Soc.* **2015,** *162* (9), A1858-A1863.
(43) Hatchard, T. D.; Obrovac, M. N.; Dahn, J. R., Electrochemical reaction of the SiZn binary system with Li. *J. Electrochem. Soc.* **2005,** *152* (12), A2335-A2344.
(44) Obrovac, M. N.; Christensen, L., Structural changes in silicon anodes during lithium insertion/extraction. *Electrochem. Solid St.* **2004,** *7* (5), A93-A96.
(45) McDowell, M. T.; Lee, S. W.; Nix, W. D.; Cui, Y., 25th Anniversary Article: Understanding the Lithiation of Silicon and Other Alloying Anodes for Lithium-Ion Batteries. *Adv. Mater.* **2013,** *25* (36), 4966-4984.
(46) Beaulieu, L. Y.; Hatchard, T. D.; Bonakdarpour, A.; Fleischauer, M. D.; Dahn, J. R., Reaction of Li with alloy thin films studied by AFM. *J. Electrochem. Soc.* **2003,** *150* (11), A1457-A1464.
(47) McDowell, M. T.; Lee, S. W.; Harris, J. T.; Korgel, B. A.; Wang, C. M.; Nix, W. D.; Cui, Y., In Situ TEM of Two-Phase Lithiation of Amorphous Silicon Nanospheres. *Nano Lett.* **2013,** *13* (2), 758-764.
(48) Gu, M.; He, Y.; Zheng, J. M.; Wang, C. M., Nanoscale silicon as anode for Li-ion batteries: The fundamentals, promises, and challenges. *Nano Energy* **2015,** *17*, 366-383.
(49) Chen, X.; Li, W. J.; Dou, S. L.; Wang, L. B.; Zhao, Y. M.; Zhang, X.; Li, Y.; Zhao, J. P., MgF as abundant and environmentally friendly electrolytes for high performance electrochromic devices. *J. Materiomics* **2021,** *7* (6), 1318-1323.

(50) He, M. F.; Guo, R.; Hobold, G. M.; Gao, H. N.; Gallant, B. M., The intrinsic behavior of lithium fluoride in solid electrolyte interphases on lithium. *P. Natl. Acad. Sci. USA* **2020,** *117* (1), 73-79.
(51) Chen, J.; Fan, X. L.; Li, Q.; Yang, H. B.; Khoshi, M. R.; Xu, Y. B.; Hwang, S.; Chen, L.; Ji, X.; Yang, C. Y.; He, H. X.; Wang, C. M.; Garfunkel, E.; Su, D.; Borodin, O.; Wang, C. S., Electrolyte design for LiF-rich solid-electrolyte interfaces to enable high-performance microsized alloy anodes for batteries. *Nat. Energy* **2020,** *5* (5), 386-397.
(52) McBrayer, J. D.; Rodrigues, M. T. F.; Schulze, M. C.; Abraham, D. P.; Apblett, C. A.; Bloom, I.; Carroll, G. M.; Colclasure, A. M.; Fang, C.; Harrison, K. L.; Liu, G.; Minteer, S. D.; Neale, N. R.; Veith, G. M.; Johnson, C. S.; Vaughey, J. T.; Burrell, A. K.; Cunningham, B., Calendar aging of silicon-containing batteries. *Nat. Energy* **2021,** *6* (9), 866-872.
(53) Mc Carthy, K.; Gullapalli, H.; Ryan, K. M.; Kennedy, T., Electrochemical impedance correlation analysis for the estimation of Li-ion battery state of charge, state of health and internal temperature. *J. Energy Storage* **2022,** *50*, 104608.
(54) Lazanas, A. C.; Prodromidis, M. I., Electrochemical Impedance Spectroscopy-A Tutorial. *ACS Meas. Sci. Au* **2023,** *3* (3), 162-193.
(55) Martin, M. H.; Lasia, A., Influence of experimental factors on the constant phase element behavior of Pt electrodes. *Electrochim. Acta* **2011,** *56* (23), 8058-8068.
(56) Kulova, T. L.; Pleskov, Y. V.; Skundin, A. M.; Terukov, E. I.; Kon'kov, O. I., Lithium intercalation into amorphous-silicon thin films: An electrochemical-impedance study. *Russ. J. Electrochem.* **2006,** *42* (7), 708-714.
(57) Laschuk, N. O.; Easton, E. B.; Zenkina, O. V., Reducing the resistance for the use of electrochemical impedance spectroscopy analysis in materials chemistry. *RSC Adv.* **2021,** *11* (45), 27925-27936.
(58) Shpigel, N.; Levi, M. D.; Aurbach, D., EQCM-D technique for complex mechanical characterization of energy storage electrodes: Background and practical guide. *Energy Storage Mater.* **2019,** *21*, 399-413.
(59) von Cresce, A.; Russell, S. M.; Baker, D. R.; Gaskell, K. J.; Xu, K., In Situ and Quantitative Characterization of Solid Electrolyte Interphases. *Nano Lett.* **2014,** *14* (3), 1405-1412.
(60) Shi, S. Q.; Lu, P.; Liu, Z. Y.; Qi, Y.; Hector, L. G.; Li, H.; Harris, S. J., Direct Calculation of Li-Ion Transport in the Solid Electrolyte Interphase. *J. Am. Chem. Soc.* **2012,** *134* (37), 15476-15487.
(61) Yang, Z. Z.; Dixon, M. C.; Erck, R. A.; Trahey, L., Quantification of the Mass and Viscoelasticity of Interfacial Films on Tin Anodes Using EQCM-D. *ACS Appl. Mater. Interfaces* **2015,** *7* (48), 26585-26594.